

# Blue-tilted Tensor Spectrum and Thermal History of the Universe

Sachiko Kuroyanagi<sup>1</sup>, Tomo Takahashi<sup>2</sup> and Shuichiro Yokoyama<sup>3</sup>

<sup>1</sup> *Department of Physics, Faculty of Science, Tokyo University of Science, 1-3, Kagurazaka, Shinjuku-ku, Tokyo 162-8601, Japan*

<sup>2</sup> *Department of Physics, Saga University, Saga 840-8502, Japan*

<sup>3</sup> *Institute for Cosmic Ray Research, University of Tokyo, Kashiwa 277-8582, Japan*

## Abstract

We investigate constraints on the spectral index of primordial gravitational waves (GWs), paying particular attention to a blue-tilted spectrum. Such constraints can be used to test a certain class of models of the early Universe. We investigate observational bounds from LIGO+Virgo, pulsar timing and big bang nucleosynthesis, taking into account the suppression of the amplitude at high frequencies due to reheating after inflation and also late-time entropy production. Constraints on the spectral index are presented by changing values of parameters such as reheating temperatures and the amount of entropy produced at late time. We also consider constraints under the general modeling approach which can approximately describe various scenarios of the early Universe. We show that the constraints on the blue spectral tilt strongly depend on the underlying assumption and, in some cases, a highly blue-tilted spectrum can still be allowed.

# 1 Introduction

Primordial gravitational waves (GWs) are one of the most important probe of the very early Universe and a lot of efforts have been made for this subject both in theoretical and observational aspects. In particular, the recent result of B-mode polarization in cosmic microwave background (CMB) from BICEP2 [1, 2] that claimed the detection of the primordial GWs has been stimulating a lot of research. Although there have been some debate regarding the issue of the foreground subtraction in BICEP2 [3–5], taking it at face value, the BICEP2 result seems to be inconsistent with the temperature data from Planck. From the analysis of Planck+WMAP 9-year polarization in the framework of the  $\Lambda$ CDM+tensor mode, the upper bound on the tensor-to-scalar ratio  $r$  has been given as  $r < 0.11$  (95 % C.L) [6], while the recent BICEP2 gives the bound  $r = 0.2_{-0.05}^{+0.07}$  (68 % C.L.) [1]. This tension motivates various works considering an extension of the standard cosmological model, one of which is a blue-tilted tensor spectrum [7–11]. Although the standard inflation model predicts a red-tilted spectrum since the tensor spectral index  $n_T$  has the so-called consistency relation  $n_T = -r/8$ , a blue-tilted spectrum can be realized in some models, e.g, string gas cosmology [12], super-inflation models [13], G-inflation [14], non-commutative inflation [15, 16], particle production during inflation [17, 18], and so on. Therefore, observational constraints on the blue-tilted tensor spectrum would be worth investigating also from the perspective of models of the early Universe.

Aside from the CMB, primordial GWs could be also detected as a stochastic GW background and there are several observational constraints on the energy density of the stochastic GWs at different GW frequencies: pulsar timing [19–22], big bang nucleosynthesis (BBN) [23, 24], interferometric GW detectors such as LIGO and Virgo [25] and so on <sup>#1</sup>. Although these limits are far above the prediction of the standard inflationary models, a strongly blue-tilted tensor spectrum can easily be excluded by these constraints, which has been investigated in [40, 41].

However, it should be noted that the thermal history of the Universe affects the spectrum of the primordial GWs [42–50]. For instance, high-frequency primordial GWs which entered the horizon during a matter-like component dominated epoch, such as that exists during reheating or late-time entropy production, have different frequency dependence compared to those which entered the radiation dominated epoch. This results in a suppression of the spectrum at high frequencies, whose range depends on when and how long it took place. It should also be noted that the above-mentioned generation mechanisms of GWs do not necessarily predict a blue-tilted spectrum over all the frequencies. The spectral index of the primordial GW spectrum can change at some frequency. Therefore,

---

<sup>#1</sup> There are more ways to obtain upper bounds on the amount of the stochastic GWs, such as dark radiation constraints from the CMB [28, 29], CMB  $\mu$  distortion [30, 31], helioseismology [32], precision Doppler tracking from the Cassini spacecraft [33], orbital monitoring of binary systems [34], torsion-bar antennas [35], seismic spectrum from the Earth [36], synchronous recycling interferometers [37], cross-correlation measurement between the Explorer and Nautilus cryogenic resonant bar detectors [38], and Global Positioning System (GPS) satellite [39].

if we also take into account the spectral shapes caused by those effects, the constraint on  $n_T$  changes depending on the underlying scenario of the early Universe, which we are going to investigate in this paper.

For this purpose, we use two different approaches to describe the GW spectrum. First, we consider constraints on  $n_T$  taking into account the suppression of the spectrum at high frequencies due to reheating and late-time entropy production, assuming that the primordial spectrum has uniform spectral index over all frequencies. For this case, we use a fitting formula which can reproduce the effect of the thermal history on the spectrum with a very good accuracy. Second, we consider the constraints on  $n_T$  without assuming an explicit model of the early Universe. Since the shape of the GW spectrum strongly depends on the model assumed, we use a more general form of the spectrum such that the spectral index changes from  $n_T$  to a different value at a given frequency. This modeling also includes the case where the Universe is dominated by a component whose equation of state differs from that of radiation/matter component. Although we assume that the transition is discontinuous, this method can approximately describe GW spectra in several scenarios of the early Universe.

This paper is organized as follows. In the next section, we begin with a brief review of the formalism to calculate the GW spectrum, taking into account the effect of thermal history by using fitting functions. In Section 3, first we summarize current observational bounds on the amplitude of the GW to be used in providing an upper bound on  $n_T$ . Then we show how the constraints on  $n_T$  change depending on the existence of reheating and late-time entropy production. Subsequently, we provide constraints on  $n_T$  under the general modeling. The final section is devoted to the conclusion of this paper.

## 2 GW spectrum and thermal history of the Universe

Here, we briefly summarize the formalism to calculate the spectrum of a stochastic GW background of primordial origin. GWs are described as a tensor part of the metric perturbation in the flat Friedmann-Robertson-Walker (FRW) background, which is given as

$$ds^2 = -dt^2 + a^2(t) (\delta_{ij} + h_{ij}(t, \mathbf{x})) dx^i dx^j = a^2(\tau) [-d\tau^2 + (\delta_{ij} + h_{ij}(\tau, \mathbf{x})) dx^i dx^j], \quad (1)$$

where  $a(\tau)$  is the scale factor and  $\tau$  is the conformal time which is related to the cosmic time  $t$  with  $d\tau = dt/a$ . The tensor metric perturbation  $h_{ij}$  satisfies the transverse-traceless condition  $\partial^i h_{ij} = h^i_i = 0$ . The energy density of GWs  $\rho_{\text{GW}}$  is given by

$$\rho_{\text{GW}} = \frac{1}{64\pi G a^2} \langle (\partial_\tau h_{ij})^2 + (\nabla h_{ij})^2 \rangle, \quad (2)$$

where the bracket indicates the spacial average. By Fourier transforming  $h_{ij}(\tau, \mathbf{x})$  as

$$h_{ij}(\tau, \mathbf{x}) = \sum_{\lambda=+, \times} \int \frac{dk^3}{(2\pi)^{3/2}} \epsilon_{ij}^\lambda h_{\mathbf{k}}(\tau) e^{i\mathbf{k}\cdot\mathbf{x}}, \quad (3)$$

with  $\epsilon_{ij}^\lambda$  being the polarization tensor, which satisfies the symmetric, transverse-traceless condition and normalized by the relation  $\sum_{i,j} \epsilon_{ij}^\lambda (\epsilon_{ij}^{\lambda'})^* = 2\delta^{\lambda\lambda'}$ , the GW energy density  $\rho_{\text{GW}}$  can be rewritten as

$$\rho_{\text{GW}} = \frac{1}{32\pi G} \int d \ln k \left( \frac{k}{a} \right)^2 \frac{k^3}{\pi^2} \sum_{\lambda} |h_{\mathbf{k}}^\lambda|^2. \quad (4)$$

Conventionally, the amplitude of GWs is characterized in the form of the energy density parameter of GWs per logarithmic interval of the wave number  $k$  <sup>#2</sup> normalized by the critical density  $\rho_{\text{crit}}(t) = 3H^2/(8\pi G)$ ,

$$\Omega_{\text{GW}}(k) \equiv \frac{1}{\rho_{\text{crit}}} \frac{d\rho_{\text{GW}}}{d \ln k}. \quad (5)$$

Using Eq. (4), we can express  $\Omega_{\text{GW}}$  as

$$\Omega_{\text{GW}}(k) = \frac{1}{12} \left( \frac{k}{aH} \right)^2 \mathcal{P}_T(k). \quad (6)$$

Here we have introduced the power spectrum  $\mathcal{P}_T(k)$  as

$$\mathcal{P}_T(k) = \frac{k^3}{\pi^2} \sum_{\lambda} |h_{\mathbf{k}}^\lambda|^2 = T_T^2(k) \mathcal{P}_T^{\text{prim}}(k), \quad (7)$$

where  $T_T(k)$  is the transfer function and  $\mathcal{P}_T^{\text{prim}}(k)$  is the primordial tensor power spectrum.  $\mathcal{P}_T^{\text{prim}}(k)$  is commonly parametrized as

$$\mathcal{P}_T^{\text{prim}}(k) = A_T(k_{\text{ref}}) \left( \frac{k}{k_{\text{ref}}} \right)^{n_T}, \quad (8)$$

where  $A_T(k_{\text{ref}})$  and  $n_T$  are the amplitude and the spectral index at the reference scale  $k_{\text{ref}}$ . The amplitude,  $A_T(k_{\text{ref}})$ , is usually characterized by the so-called tensor-to-scalar ratio  $r$  defined by

$$r(k_{\text{ref}}) \equiv \frac{\mathcal{P}_T^{\text{prim}}(k_{\text{ref}})}{\mathcal{P}_\zeta(k_{\text{ref}})}, \quad (9)$$

and we have

$$A_T(k_{\text{ref}}) = r \mathcal{P}_\zeta(k_{\text{ref}}), \quad (10)$$

where  $\mathcal{P}_\zeta(k_{\text{ref}})$  is the power spectrum for the scalar perturbation and it is precisely measured as  $\mathcal{P}_\zeta = 2.2 \times 10^{-9}$  at  $k_{\text{ref}} = 0.01 \text{Mpc}^{-1}$  [6].

---

<sup>#2</sup> In the later part of the paper, we also use frequency  $f = k/2\pi$  instead of  $k$ .

The transfer function  $T_T(k)$  describes the evolution of GWs after horizon crossing, which depends on the thermal history of the Universe. This can be obtained by numerically solving the evolution equation of the GWs:

$$h''_{ij} + 2aHh'_{ij} - \nabla^2 h_{ij} = 0, \quad (11)$$

where a prime denotes a derivative with respect to the conformal time. In the following subsections, we provide fitting formulas which enable us to easily express the effects of thermal history with a few parameters.

## 2.1 Standard reheating scenario

Let us first consider the standard reheating scenario in which soon after inflation the Universe has matter-dominated (MD) like phase before the completion of reheating. Such a phase is preceded by the oscillation of inflaton field at the bottom of its quadratic potential. After the completion of reheating, the Universe becomes radiation-dominated (RD). In such a case, the transfer function is described as [45, 48, 49, 51, 52]:

$$T_T^2(k) = \Omega_m^2 \left( \frac{g_*(T_{\text{in}})}{g_{*0}} \right) \left( \frac{g_{*s0}}{g_{*s}(T_{\text{in}})} \right)^{4/3} \left( \frac{3j_1(k\tau_0)}{k\tau_0} \right)^2 T_1^2(x_{\text{eq}}) T_2^2(x_R), \quad (12)$$

where  $j_\ell(k\tau_0)$  is the  $\ell$ th spherical Bessel function, given by  $j_1(k\tau_0) = 1/(\sqrt{2}k\tau_0)$  in the limit of  $k\tau_0 \rightarrow 0$ . The subscript “0” indicates that the quantity is evaluated at the present time. The values of the relativistic degrees of freedom  $g_*(T_{\text{in}})$  and its counterpart for entropy  $g_{*s}(T_{\text{in}})$  change depending on  $T_{\text{in}}(k)$ , which is the temperature of the Universe when the mode  $k$  enters the horizon, and affects the spectral amplitude of the mode [53]<sup>#3</sup>. The index  $i$  in  $x_i \equiv k/k_i$  corresponds to the transition epoch of the Hubble expansion rate. The wavenumbers corresponding to the matter-radiation equality and the completion of reheating are respectively given by

$$k_{\text{eq}} = 7.1 \times 10^{-2} \Omega_m h^2 \text{ Mpc}^{-1}, \quad (13)$$

$$k_R = 1.7 \times 10^{14} \left( \frac{g_{*s}(T_R)}{106.75} \right)^{1/6} \left( \frac{T_R}{10^7 \text{ GeV}} \right) \text{ Mpc}^{-1}. \quad (14)$$

For  $T_1^2(x)$  and  $T_2^2(x)$ , we use the following fitting functions,

$$T_1^2(x) = 1 + 1.57x + 3.42x^2, \quad (15)$$

$$T_2^2(x) = (1 - 0.22x^{1.5} + 0.65x^2)^{-1}. \quad (16)$$

---

<sup>#3</sup> To incorporate this effect in the GW spectrum, we introduce the following fitting function:

$$g_*(T_{\text{in}}(k)) = g_{*0} \left\{ \frac{A + \tanh \left[ -2.5 \log_{10} \left( \frac{k/2\pi}{2.5 \times 10^{-12} \text{ Hz}} \right) \right]}{A + 1} \right\} \left\{ \frac{B + \tanh \left[ -2.0 \log_{10} \left( \frac{k/2\pi}{6.0 \times 10^{-9} \text{ Hz}} \right) \right]}{B + 1} \right\}$$

where  $A = (-1 - 10.75/g_{*0})/(-1 + 10.75/g_{*0})$  and  $B = (-1 - g_{\text{max}}/10.75)/(-1 + g_{\text{max}}/10.75)$ . For  $g_{\text{max}}$ , we assume the sum of the standard-model particles,  $g_{\text{max}} = 106.75$ . The same formula can be used for the counterpart for entropy  $g_{*s}(T_{\text{in}})$  by replacing  $g_{*0} = 3.36$  with  $g_{*s0} = 3.91$ .

Note that the fitting formula for  $T_2^2(x)$  is improved from [45] by changing the power of the power index of the second term. Using least-square algorithm, the power index and coefficients are readjusted to fit the spectrum obtained by numerically solving Eq. (11). (For the details of the numerical calculation, see [46].) <sup>#4</sup>

## 2.2 Late-time entropy production scenario

We also consider the case with late-time entropy production, in which the oscillation energy of another scalar field  $\sigma$  dominates the Universe some time after reheating. In some cases, during the RD era after the decay of inflaton, the oscillating  $\sigma$  field can dominate over the radiation energy density. Then, the Universe enters a MD-like phase due to the  $\sigma$  oscillation, <sup>#5</sup> and after the  $\sigma$ -field decays into radiation, the Universe is dominated by the radiation energy again. For this case, the fitting formula for the transfer function is given by [48]

$$T_T^2(k) = \Omega_m^2 \left( \frac{g_*(T_{\text{in}})}{g_{*0}} \right) \left( \frac{g_{*s0}}{g_{*s}(T_{\text{in}})} \right)^{4/3} \left( \frac{3j_l(k\tau_0)}{k\tau_0} \right)^2 T_1^2(x_{\text{eq}}) T_2^2(x_\sigma) T_3^2(x_{\sigma R}) T_2^2(x_{RF}), \quad (17)$$

where  $k_\sigma$  corresponds to the time when  $\sigma$  decays into radiation after  $\sigma$ -dominated MD-like phase, and given in the same form as Eq. (14),

$$k_\sigma = 1.7 \times 10^{14} \left( \frac{g_{*s}(T_\sigma)}{106.75} \right)^{1/6} \left( \frac{T_\sigma}{10^7 \text{ GeV}} \right) \text{ Mpc}^{-1}, \quad (18)$$

with  $T_\sigma$  being the temperature of the Universe at the  $\sigma$  decay. To write down  $k_{\sigma R}$  and  $k_{RF}$ , first we define the quantity which represents the amount of entropy production by the decay of  $\sigma$  as

$$F \equiv \frac{s(T_\sigma) a^3(T_\sigma)}{s(T_R) a^3(T_R)}, \quad (19)$$

where  $s(T)$  is the entropy density at temperature  $T$ . With this quantity, the other characteristic frequencies can be expressed as  $k_{\sigma R} = k_\sigma F^{2/3}$  and  $k_{RF} = k_R F^{-1/3}$ . The third transfer function  $T_3(x)$  describes the transition from the first RD phase to  $\sigma$ -dominated MD-like phase and we use

$$T_3^2(x) = 1 + 0.59x + 0.65x^2. \quad (20)$$

---

<sup>#4</sup> Note that, since  $x_R$  includes  $T_R$ , the coefficients will be modified depending on the definition of  $T_R$  in terms of the decay rate of the inflaton  $\Gamma$ . Numerical results are obtained for a given value of  $\Gamma$ , not  $T_R$ , and we relate these quantities by using the formula  $T_R = (10/\pi^2)^{1/4} g_*(T_R)^{-1/4} \sqrt{\Gamma M_{\text{pl}}}$  with  $M_{\text{pl}} = (8\pi G)^{-1/2}$  being the reduced Planck mass.

<sup>#5</sup> When the energy density of the  $\sigma$ -field starts to dominate the Universe, the  $\sigma$ -field is not necessarily oscillating. If the field is frozen by the Hubble friction, the Universe experiences a second inflationary phase and the amplitude of GWs at the scales which enter the horizon during this phase, is suppressed more quickly than in the case of MD-like phase [54]. Here, we focus on only MD-like phase during  $\sigma$ -dominated Universe, but it would be easy to extend our analysis to the case with such a second inflationary phase.

Note that  $T_1(x)$  is used instead of  $T_3(x)$  in [48]. In this paper, we introduce a new function  $T_3(x)$  in order to improve the fitting.

In Fig. 1, we show the spectra from the fitting formula (17), and the numerical calculation. As seen from the figure, our fitting formula well approximates the one from the numerical calculation. We note here that our new transfer functions  $T_2(x)$  and  $T_3(x)$  are also aimed to reduce a small bump around the bending point, which arises in the fitting formulas of [48] for small  $F$ . However, even with the improved formulas, as seen in the right panel of Fig. 1, a bump is unavoidable for  $F \lesssim 10$  because the frequency transitions described by  $T_2(x)$  and  $T_3(x)$  overlap with each other in a narrow frequency range. The bump can be removed by omitting the second term of  $T_3(x)$ , namely  $0.59x$  as shown in the right panel of Fig. 1. In the following analysis, we omit this term for  $F \lesssim 10$ .

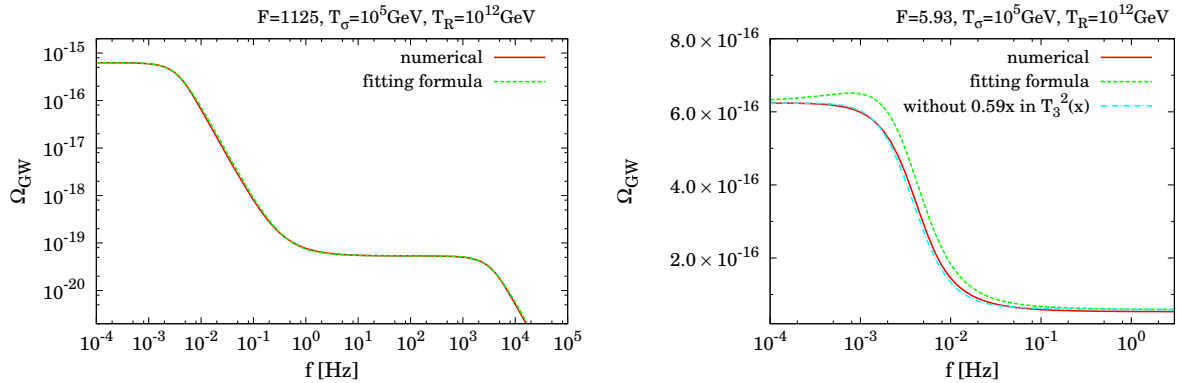


Figure 1: Comparison of spectra derived from the fitting formula (17) and numerical calculation for  $F = 1125$  (left) and  $F = 5.93$  (right). In the right panel, the spectra are plotted in linear scale and we also show the spectrum using the fitting function without the term  $0.59x$  of  $T_3(x)$  in Eq. (17), which causes an artificial bump for small  $F$ . In both figures, we assume  $r = 0.2$  and  $n_T = 0$ .

### 3 Constraints on the tensor spectral index

#### 3.1 Current observational bounds on GWs

First, we summarize observational bounds on the energy density of the stochastic GWs, which are used to obtain constraints on  $n_T$ . Among various upper bounds reported in the literature, we adopt stringent ones from interferometric GW detectors, pulsar timing array, and BBN.

### 3.1.1 Interferometric GW detectors such as LIGO+Virgo

From interferometric GW detectors such as LIGO, non-detection of GWs gives an upper bound on the stochastic GWs. In this paper, we adopt the 95 % C.L. upper bound from the LIGO-Virgo collaboration [25]<sup>#6</sup>:

$$\Omega_{\text{GW}} h^2 < 2.6 \times 10^{-6} \quad [f = 41.5 - 169.25 \text{ Hz}], \quad (21)$$

where  $h$  is the dimensionless Hubble parameter which parametrizes the present Hubble constant as  $H_0 = 100h \text{ km/s/Mpc}$ . The analysis is performed using the approximate form of the GW spectrum,  $\Omega_{\text{GW}}(f) = \Omega_{\text{GW},\alpha}(f/100\text{Hz})^\alpha$ , where  $\alpha$  is the local power index around the sensitive frequency band  $\sim 100\text{Hz}$ , and Eq. (21) is obtained assuming  $\alpha = 0$ . The limit changes for different values of  $\alpha$ , and we describe its  $\alpha$  dependence as

$$\Omega_{\text{GW},\alpha} h^2 < 2.6 \times 10^{-6} \sqrt{\frac{5-2\alpha}{5}} \left( \frac{f_{\text{min}}}{100\text{Hz}} \right)^{-\alpha}. \quad (22)$$

This formula is obtained by adopting the approximations described below. The signal-to-noise ratio for the analysis of stochastic GWs is given by [26]

$$SNR^2 = \left( \frac{3H_0^2}{10\pi^2} \right)^2 2T_{\text{obs}} \int_{f_{\text{min}}}^{f_{\text{max}}} df \frac{\gamma_{ij}^2(f) \Omega_{\text{GW}}^2(f)}{f^6 P_i(f) P_j(f)}, \quad (23)$$

where  $T_{\text{obs}}$  is the observation time. Assuming that the overlap reduction function  $\gamma_{ij}^2(f)$  and the noise power spectral density  $P_{i,j}(f)$  have no frequency dependence, which is a reasonable assumption between  $f_{\text{max}} = 41.5 \text{ Hz}$  and  $f_{\text{min}} = 169.25 \text{ Hz}$ , we obtain  $SNR^2 \sim A^2 \Omega_{\text{GW},\alpha}^2 (f_{\text{min}}/100\text{Hz})^{2\alpha} / [(5-2\alpha)f_{\text{min}}^5]$ , where  $A^2 \equiv (3H_0^2/10\pi^2)^2 2T_{\text{obs}} \gamma_{ij}^2 / (P_i P_j)$  and we have used  $f_{\text{min}}^{2\alpha-5} \gg f_{\text{max}}^{2\alpha-5}$  for  $2\alpha - 5 < 0$ . This approximation holds in our investigation where the value of  $\alpha$  ranges from  $-2$  to  $1.6$ . Assuming a Gaussian likelihood, the bound is  $\Omega_{\text{bound},\alpha} \propto \Delta\Omega_{\text{GW},\alpha} \propto 1/SNR$  [27]. Using that the bound for  $\alpha = 0$  is  $\Omega_{\text{bound},0} \propto \sqrt{5f_{\text{min}}^5}/A$ , we obtain

$$\Omega_{\text{bound},\alpha} = \frac{\sqrt{(5-2\alpha)f_{\text{min}}^5}}{A} \left( \frac{f_{\text{min}}}{100\text{Hz}} \right)^{-\alpha} = \Omega_{\text{bound},0} \sqrt{\frac{5-2\alpha}{5}} \left( \frac{f_{\text{min}}}{100\text{Hz}} \right)^{-\alpha}, \quad (24)$$

which gives Eq. (22).

### 3.1.2 Pulsar timing array

We also adopt the upper bound from pulsar timing array. Using millisecond pulsars as very precise clocks, GWs can be searched through the effect on the pulse arrival timings,

---

<sup>#6</sup> In [25], the bounds on the GW amplitude for the frequency regions  $f = 600\text{--}1000 \text{ Hz}$  and  $1000\text{--}1726 \text{ Hz}$  are also given. Although these bounds may be able to constrain very blue-tilted spectrum, we checked that these bounds are irrelevant in the parameter regions which we explore in our analysis. Thus we only consider the bound for  $f = 41.5\text{--}169.25 \text{ Hz}$  in the following analysis.

which currently provides the stringent constraint on the amplitude of GWs at  $f \sim 10^{-8}$  Hz. Among several bounds reported so far, we use the recent one obtained from the North American Nanohertz Observatory for Gravitational waves (NANOGrav) project [21], which gives the upper bound:

$$\Omega_{\text{GW}} h^2 < 1.1 \times 10^{-8} \quad [f = 1/(5.54 \text{ years}) = 5.72 \times 10^{-9} \text{ Hz}], \quad (25)$$

In [21], GW spectrum is modeled by  $h_c(f) = A_{1\text{year}}(f/f_{1\text{year}})^\beta$ , which corresponds to the energy density as  $\Omega_{\text{GW}}(f) = (2\pi^2/3H_0^2)f^2 h_c^2(f)$ , and the spectral index dependence of the upper bound is found to be well approximated by  $A_{1\text{year}} = 2.26 \times 10^{-14}(5.54\text{year}/1\text{year})^\beta$ . This dependence can be canceled by choosing the reference frequency to be  $f = 1/(5.54\text{years}) = 5.72 \times 10^{-9}\text{Hz}$ . Then the bound becomes

$$h_c(f_{5.54\text{year}}) < 2.26 \times 10^{-14} \left( \frac{5.54\text{year}}{1\text{year}} \right)^\beta \left( \frac{f_{5.54\text{year}}}{f_{1\text{year}}} \right)^\beta = 2.26 \times 10^{-14}, \quad (26)$$

from which we obtain the bound Eq. (25).

### 3.1.3 Big Bang Nucleosynthesis (BBN)

We also consider constraints from BBN. Primordial GWs contribute to the energy density of the Universe as an extra radiation component. Such an extra radiation component changes the expansion rate of the Universe during BBN and affects the abundance of the light elements. The total energy density of GWs, given by integrating the density parameter  $\Omega_{\text{GW}}(f)$ , is therefore constrained not to spoil BBN [23, 24]:

$$\int_{f_1}^{f_2} d(\ln f) \Omega_{\text{GW}}(f) h^2 \leq 5.6 \times 10^{-6} (N_{\text{eff}}^{(\text{upper})} - 3), \quad (27)$$

where  $N_{\text{eff}}^{(\text{upper})}$  is the upper bound on the effective number of extra radiation at the time of BBN. The lower limit of the integral in the left hand side is given by the frequency which corresponds to the comoving horizon at the time of BBN and we take  $f_1 = 10^{-10}$  Hz. For the upper cutoff, we take  $f_2 = 10^7$  Hz, which corresponds to the temperature of the Universe  $\sim 10^{15}$  GeV. Recent analysis gives the constraint on the extra radiation component as  $N_{\text{eff}} = 3.71_{-0.45}^{+0.49}$  at  $1\sigma$  C.L. [55]. We adopt the 95 % C.L. upper limit of  $N_{\text{eff}}^{(\text{upper})} = 4.65$  in the following analysis. In the appendix, we provide analytic estimate of the upper bounds on  $n_T$ , and show its dependence on the reheating temperature  $T_R$ .

## 3.2 Results

First, to illustrate how the above observational bounds on  $\Omega_{\text{GW}}(f)$  help to provide upper bounds on  $n_T$  in consideration of the reheating and late-time entropy production, in Fig. 2, we show spectra of the stochastic GW background for different thermal history together

with the observational bounds. As seen from the figure, large values of  $n_T$  can elude the observational constraints if the reheating temperature is low or the amount of entropy produced at late time is large.

In the following, we investigate constraints on  $n_T$  for the cases of the standard reheating and late-time entropy production scenarios, and show how the constraint depends on parameters characterizing the thermal history such as  $T_R, T_\sigma$  and  $F$ . We fix the tensor-to-scalar ratio at the reference scale  $k_{\text{ref}} = 0.01\text{Mpc}^{-1}$  to be  $r = 0.2$  in the following analysis.

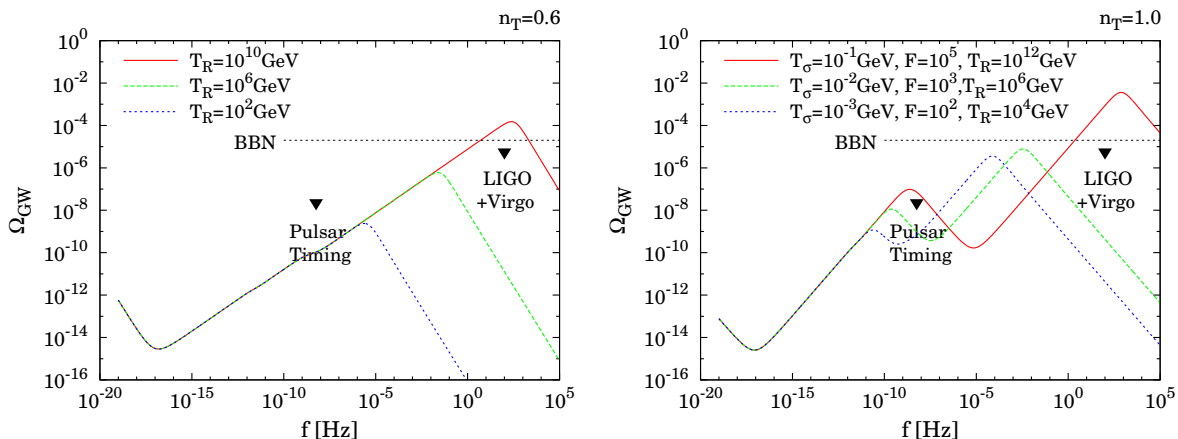


Figure 2: The GW spectra for the cases with the standard thermal history (left) and entropy production due to the decay of the  $\sigma$ -field (right). In the left panel, spectra with  $n_T = 0.6$  are shown by changing reheating temperature  $T_R$ . In the right panel, spectra with  $n_T = 1.0$  are shown for different values of  $T_R, T_\sigma$  and  $F$ . In both figures, we assume  $r = 0.2$ .

### 3.2.1 Case with the standard reheating scenario

We first consider the case of the standard reheating scenario. In this scenario, the Universe enters the MD-like epoch soon after the end of inflation, and is connected to the RD phase when the temperature of the Universe becomes  $T = T_R$ . In some models, the thermal history may be different from the standard one assumed here, but in such a case, we can apply constraints for a more general case which will be discussed in Sec. 3.3. For given  $n_T$  and  $T_R$ , we calculate the stochastic GW spectrum with the method described in Sec. 2 and compare it with the current observational bounds, Eqs. (21), (25) and (27).

In Fig. 3, we show the parameter space ruled out by LIGO, pulsar timing and BBN in the  $n_T - T_R$  plane. As for the constraints from the LIGO and pulsar timing, we find a characteristic temperature above which the constraint on  $n_T$  does not depend on the reheating temperature. This is because, the reheating temperature characterizes the frequency of the suppression due to reheating as seen in Fig. 2, and determine the peak

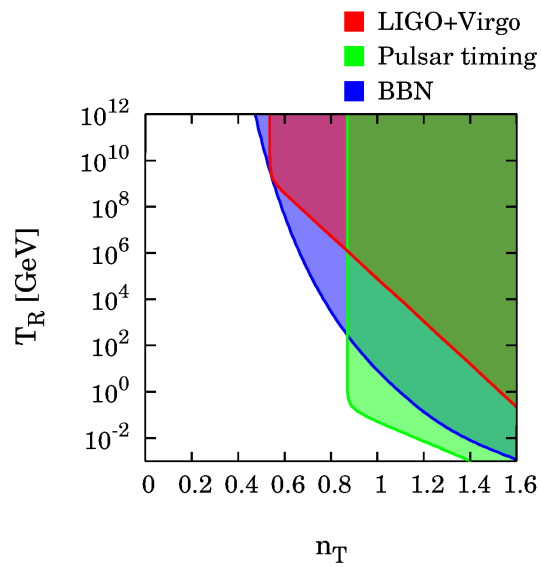


Figure 3:  $2\sigma$  excluded region (colored) in the  $n_T$ - $T_R$  plane for the case of the standard reheating scenario. The tensor-to-scalar ratio is assumed to be  $r = 0.2$ .

frequency of the spectrum (for  $0 < n_T < 2$ ). For a reheating temperature higher than a certain value, the suppression occurs at the frequencies higher than the frequency band of the experiment, and the observational bound on  $n_T$  is determined regardless of the effect of reheating. In contrast, for a lower reheating temperature, the effect of reheating becomes important at the frequency of the experiment, and the constraint on  $n_T$  is weakened for smaller  $T_R$ . The BBN can put a relatively severe constraint on  $n_T$  depending on the reheating temperature. This is because the bound is subject to the integrated value given in Eq. (27). By putting together all the constraints, we see the tendency that the constraint on  $n_T$  is relaxed for lower reheating temperatures. In order not to spoil the success of BBN, demanding that the reheating temperature should be larger than about 10 MeV, which indicates that the spectral index  $n_T$  should be smaller than 1.2 for  $r = 0.2$ .

### 3.2.2 Case with late-time entropy production scenario

Next, we consider the case with late-time entropy production scenario. If large entropy is produced by the decay of another scalar field  $\sigma$ , the GW spectrum is further suppressed as illustrated in the right panel of Fig. 2. The degree of the suppression depends on the amount of the entropy produced, which is characterized by the quantity  $F$  defined in Eq. (19). The frequency range of the suppression depends on the temperature of the Universe at the end of the second reheating  $T_\sigma$ . Therefore, the bound on  $n_T$  depends on both  $F$  and  $T_\sigma$ . While it also depends on the reheating temperature  $T_R$  as seen in Fig. 2, here we focus on the parameters characterizing the late-time entropy production,  $F$  and  $T_\sigma$ . Hence, we fix the reheating temperature  $T_R$  to be rather high as  $T_R = 10^{15}$  GeV in order not to include the effect of the first reheating in the constraints on  $n_T$  and to simply see the tendency of the effect of the late-time entropy production.

To see the parameter dependence of the constraint, we show excluded parameter space in the  $n_T$ - $F$  and  $n_T$ - $T_\sigma$  planes in Figs. 4 and 5, respectively. First, in Fig. 4,  $T_\sigma$  is fixed to be  $10^{-2}$  GeV (left panel) and  $10^3$  GeV (right panel). Since a larger value of  $F$  gives a larger suppression of the GW spectrum, constraints from LIGO and BBN on  $n_T$  are weakened as  $F$  becomes large. On the other hand, especially in the right panel, we see the upper bound on  $n_T$  obtained from pulsar timing does not depend on the value of  $F$ . This is because the constraint from pulsar timing is put at  $f \sim 10^{-8}$  Hz, which corresponds to the mode who entered the horizon at  $T \sim 1$  GeV. Thus, for the case of  $T_\sigma > 1$  GeV, the spectrum is suppressed at frequencies higher than  $f \sim 10^{-8}$  Hz and thus the constraint from pulsar timing is irrelevant to the value of  $F$ .

In Fig. 5, we show the constrains in the  $n_T$ - $T_\sigma$  plane by fixing the value of  $F$  to be  $10^2$  and  $10^5$ . Since  $T_\sigma$  determines the frequency of the suppression, the tendency is expected to be similar to that of  $T_R$  obtained in Sec. 3.2.1 for the standard reheating scenario. However, in contrast to the case of the standard reheating scenario, we find that the constraints on  $n_T$  from LIGO and BBN do not change depending on the value of  $T_\sigma$ . The reason is that the suppression due to late-time entropy production arises in a certain range of frequency, which is determined by the amount of entropy production  $F$ , and the spectrum becomes

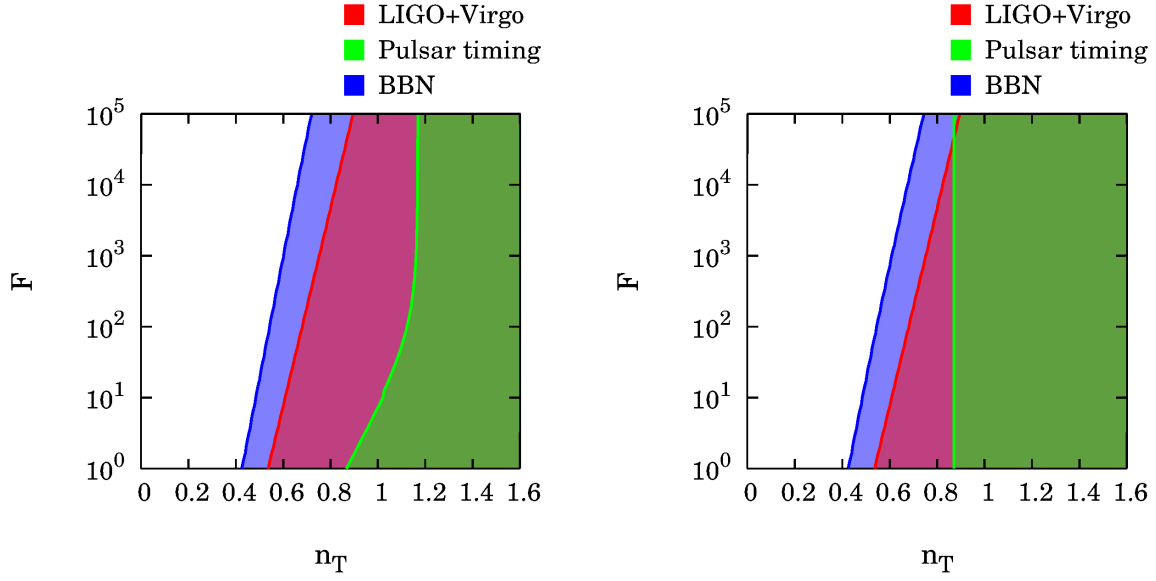


Figure 4:  $2\sigma$  excluded region (colored) in the  $n_T$ - $F$  plane for the cases of  $T_\sigma = 10^{-2}$  GeV (left) and  $10^3$  GeV (right). We assume  $r = 0.2$  and  $T_R = 10^{15}$  GeV.

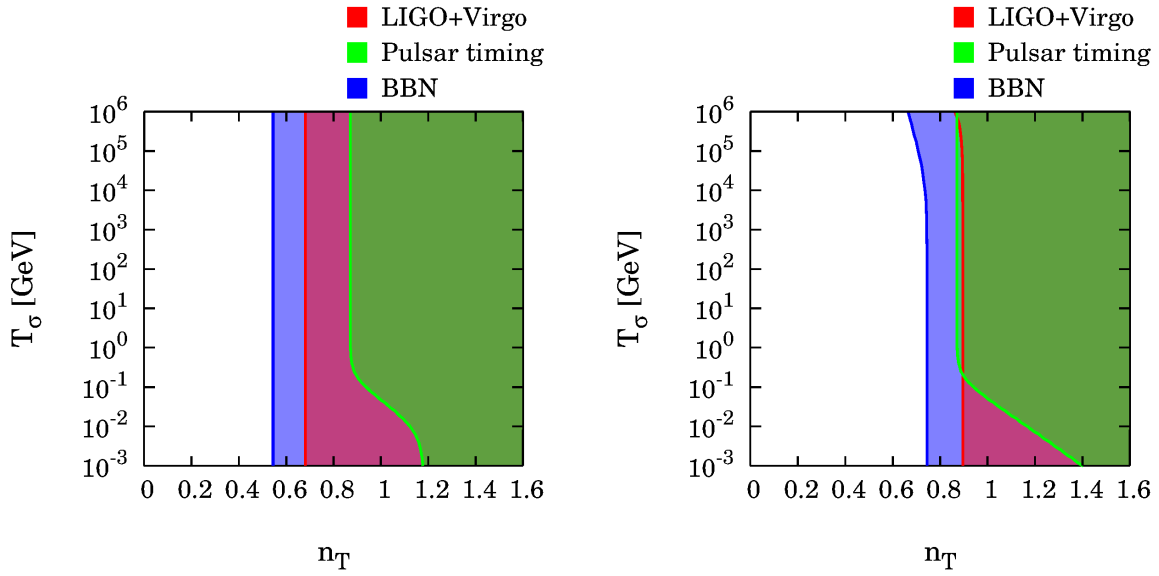


Figure 5:  $2\sigma$  excluded region (colored) in the  $n_T$ - $T_\sigma$  plane for the cases of  $F = 10^2$  (left) and  $10^5$  (right). We assume  $r = 0.2$  and  $T_R = 10^{15}$  GeV.

blue again at high frequency. The values  $F = 10^2$  and  $10^5$  assumed here are not enough to reduce the GW amplitude at high frequency and to relax the observational bound. Note that since we assume  $T_R = 10^{15}$  GeV, the blue-tilted spectrum continues to rise towards high frequencies. This results in the strong constraint from BBN, since the BBN bound is valid even at very high frequency.

As we have seen in Figs. 4 and 5, once the parameters  $T_\sigma$ ,  $F$ ,  $T_R$  and  $r$  are fixed, we can obtain an upper bound on  $n_T$ . In Fig. 6, we show contours of the  $2\sigma$  upper bound value of  $n_T$  in the  $T_\sigma$ - $F$  plane for each observational constraint, by fixing the other parameters as  $T_R = 10^{15}$  GeV and  $r = 0.2$ . Since LIGO is sensitive at high frequency  $f \sim 100$  Hz, as far as  $T_\sigma < 10^{10}$  GeV, the upper bound on  $n_T$  does not depend on  $T_\sigma$ , and only be affected by the value of  $F$ . On the other hand, the pulsar timing has sensitivity at relatively low frequency  $f \sim 10^{-8}$  Hz. When  $T_\sigma$  is below  $\mathcal{O}(0.1)$  GeV, the suppression becomes important at  $f \sim 10^{-8}$  Hz, and we see the upper bound on  $n_T$  is indeed weakened. From the figure, we can see that BBN provides a stringent upper bound on  $n_T$  in most parameter space. One of the reason is that, the reheating temperature is assumed to be very high  $T_R = 10^{15}$  GeV and the spectrum is not suppressed by reheating, which enables the BBN to put strong constraint at very high frequency region. If we take a lower value for  $T_R$ , the BBN constraint becomes less stringent.

### 3.3 Extension to more general case

In the last subsection, we study the more general case where the stochastic GW spectrum is modeled by two parameters  $\alpha$  and  $f_\alpha$ , such that the power index of the spectrum changes from  $n_T$  to  $\alpha$  at a characteristic frequency  $f_\alpha$ . This modeling covers a broad class of models of the early Universe, and enables us to provide more general discussions. For example, one can interpret the change of the power-law behavior as an effect of the change of the background evolution, which is applicable not only for reheating but also for different models (e.g. kination dominated phase). One can also adjust parameter values to describe particular generation mechanism of primordial GWs which does not predict a uniform spectral index over whole frequency range.

Here we model the GW spectrum as

$$\Omega_{\text{GW}}(k) = \begin{cases} \frac{1}{12} \left( \frac{k}{aH} \right)^2 T_T^2(k) A_T(k_{\text{ref}}) \left( \frac{k}{k_{\text{ref}}} \right)^{n_T} & (k < k_\alpha), \\ \frac{1}{12} \left( \frac{k}{aH} \right)^2 T_T^2(k) A_T(k_{\text{ref}}) \left( \frac{k_\alpha}{k_{\text{ref}}} \right)^{n_T} \left( \frac{k}{k_\alpha} \right)^\alpha & (k > k_\alpha), \end{cases}$$

where  $k_\alpha$  is the frequency at which the power index of the spectrum changes from  $n_T$  to  $\alpha$ . The corresponding frequency  $f_\alpha$  is given by  $f_\alpha = k_\alpha/2\pi$ . Here, we assume that  $T_T^2(k)$  includes only  $T_1^2(k)$ , not  $T_2^2(k)$  and  $T_3^2(k)$ , which means that the change of the frequency dependence due to matter-radiation equality is included, but the effect of reheating and late-time entropy production is not included in the transfer function.

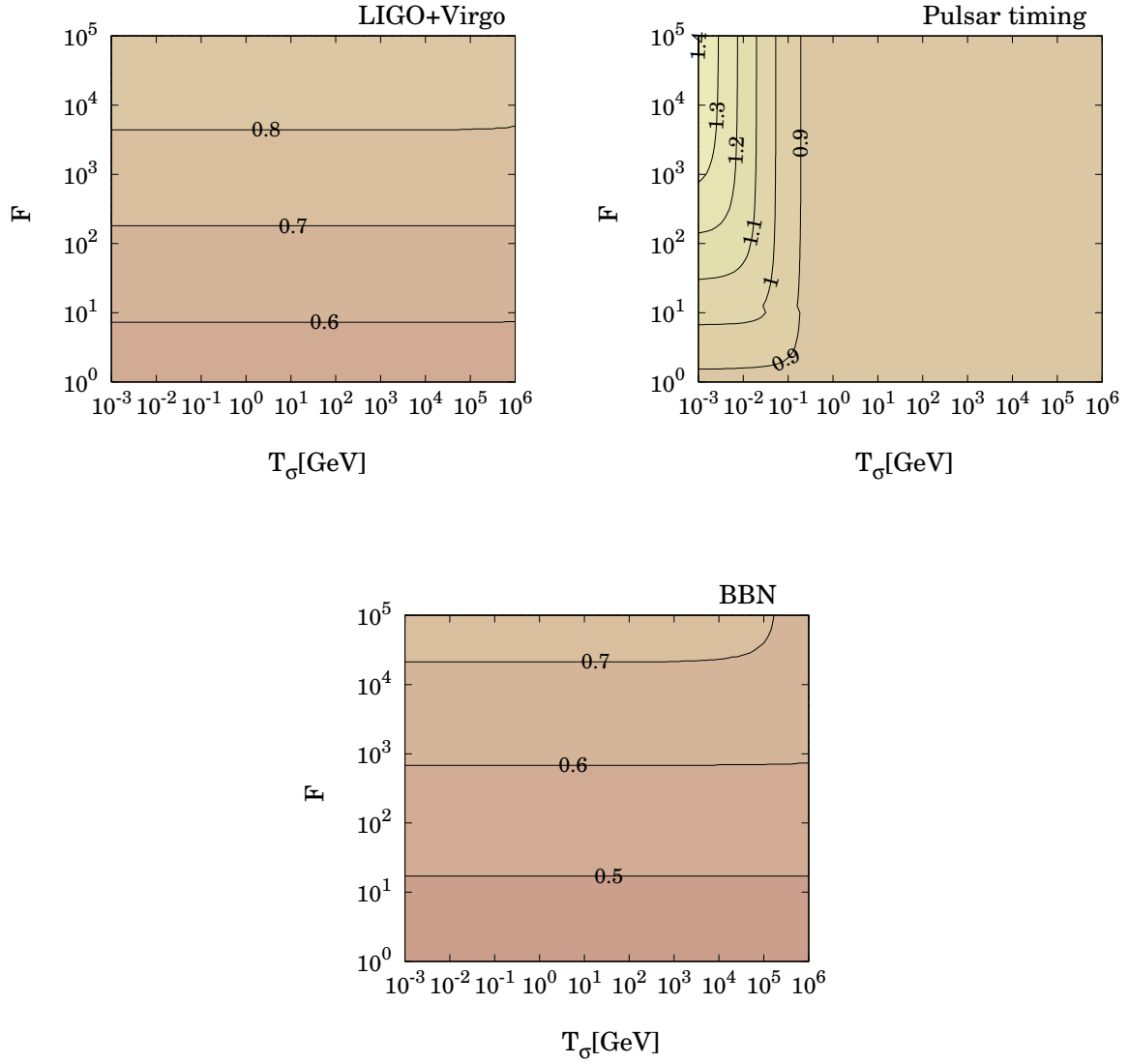


Figure 6: Contours of the upper bound on  $n_T$  in the  $T_\sigma$ - $F$  plane obtained from LIGO (top left), pulsar timing (top right) and BBN (bottom). Here,  $r = 0.2$  and  $T_R = 10^{15}$  GeV is assumed.

The advantage of this modeling is that it can accommodate the change of the expansion rate before the BBN epoch in a general way. For example, we can reproduce the spectrum for the standard reheating scenario by choosing  $\alpha$  to be  $-2 + n_T$  and  $f_\alpha$  to be the same as  $f_R = k_R/2\pi$ , given in Eq. (14). <sup>#7</sup>In the case where the kinetic energy of the scalar field dominates the Universe, it is known that the expansion rate evolves as  $H^2 \propto a^{-6}$  and the spectrum of GW has a frequency dependence of  $\Omega_{\text{GW}} \propto f$  [56]. Generally, assuming that the Universe is dominated by a fluid whose equation of state is  $w$ . GWs which enter the horizon during that phase have a spectral power dependence of

$$\Omega_{\text{GW}} \propto k^{\frac{2(3w-1)}{1+3w}}. \quad (28)$$

Therefore, when the background equation of state changes from  $w$  to  $1/3$  (radiation) at the temperature  $T_\alpha$ , one can describe the GW spectrum by assuming  $\alpha$  as

$$\alpha = \frac{2(3w-1)}{1+3w} + n_T, \quad (29)$$

and  $f_\alpha$  would be the quantity determined by  $T_\alpha$ .

In addition, in some models predicting a blue-tilted GW spectrum, the generation mechanism of the primordial GWs does not continuously generate a blue-tilted spectrum, and the spectral index changes from blue-tilted one to another. The general modeling is useful to describe such change of the spectral power dependence in the primordial spectrum  $\mathcal{P}_T^{\text{prim}}(k)$ . For example, if there exists some phase during inflation in which the production of the vector quanta becomes effective, for the modes which exit the horizon during such phase, the generated primordial GWs can be blue-tilted [17, 18]. This model is based on the action such as  $\frac{\psi}{4f} F_{\mu\nu} \tilde{F}^{\mu\nu}$  where  $F_{\mu\nu}$  and  $\tilde{F}^{\mu\nu} = \epsilon^{\mu\nu\alpha\beta} F_{\alpha\beta}$  are the field strength of the gauge field and its dual,  $\psi$  is a dynamical pseudo-scalar field and  $f$  is a pseudo-scalar decay constant. Through the coupling between the pseudo-scalar and gauge field, time dependent pseudo-scalar  $\psi$  induces the production of the gauge quanta and this gauge quanta becomes the source of the gravitational waves. Since the spectral tilt of the gravitational waves depends on the time evolution of the pseudo-scalar  $\psi$ , the blue tensor spectrum can be realized by taking into account appropriate dynamics of  $\psi$ . For the modes which cross the horizon after the production phase (e.g.,  $\psi$  stops the rolling), the GW spectrum is not blue-tilted anymore, and the amplitude of the primordial GWs decreases at higher frequency. In a such case, the characteristic frequency  $f_\alpha$  represents the mode which exits the horizon at the end of the effective particle creation phase during inflation. Then, the duration of the particle creation phase, measured from the time when the reference scale exit the horizon, can be expressed in terms of the  $e$ -folding number as

$$\Delta N_{\text{p.c.}} \equiv \ln \left( \frac{a_\alpha}{a_{\text{ref}}} \right) \simeq \ln \left( \frac{k_\alpha}{k_{\text{ref}}} \right), \quad (30)$$

---

<sup>#7</sup> The transfer functions  $T_2^2(k)$  and  $T_3^2(k)$  are obtained by taking into account the decay of the inflaton by following the equation of motion as well as the evolution of the Hubble parameter. Hence, the GW spectrum given by this modeling does not describe the smooth transition in the same way as the transfer functions do, but still useful as an approximated form of the spectrum.

where we assume that the Hubble parameter during inflation stays almost constant.

To obtain an intuitive idea of this modeling and how the constraint on  $n_T$  depends on the value of  $\alpha$  and  $k_\alpha$  (or  $f_\alpha$ ), we show the GW spectrum represented by Eq. (28) in Fig. 7. In this figure, we show three examples of GW spectrum considering different scenarios of the early Universe. The green dashed spectrum corresponds to a blue-tilted primordial spectrum,  $n_T = 0.6$ , which underwent the standard reheating scenario with  $T_R = 10^6$  GeV. The blue dotted one describes a scale-invariant primordial spectrum which has experienced a kination-dominated phase after inflation. For the red solid one, we consider a primordial spectrum such that the model predicts a strongly blue-tilted spectrum of  $n_T = 1$  around the CMB scale, but at some later stage, the situation become the same as the standard slow-roll inflation.

Finally, in Fig. 8, the upper bound on  $n_T$  is shown as a contour plot in the  $f_\alpha$ - $\alpha$  plane for each observation, i.e., LIGO, pulsar timing and BBN. Once we know an approximated form of the GW spectrum for some particular model, we can find the values of  $\alpha$  and  $f_\alpha$  for that model and read off the upper bound on  $n_T$  from the figure. In the figure, we can see the tendency that the constraint on  $n_T$  becomes tighter for larger  $\alpha$ , since a positive value of  $\alpha$  enhances the spectral amplitude at high frequencies. For negative values of  $\alpha$ , we can see the constraint becomes weaker when  $f_\alpha$  is smaller than the frequency of the observational bound. This is because, for smaller  $f_\alpha$ , a negative value of  $\alpha$  reduces the spectral amplitude at the corresponding frequency of the experiment. On the other hand, for larger  $f_\alpha$ , the suppression occurs at higher frequency and does not affect the spectrum at the frequency where the observational bounds are relevant.

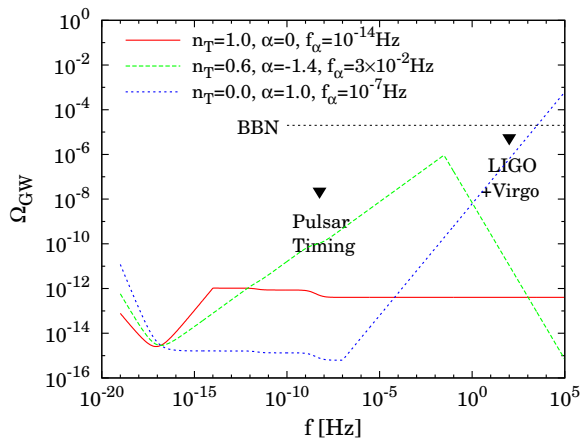


Figure 7: GW Spectra modeled by  $\alpha$  and  $f_\alpha$ .

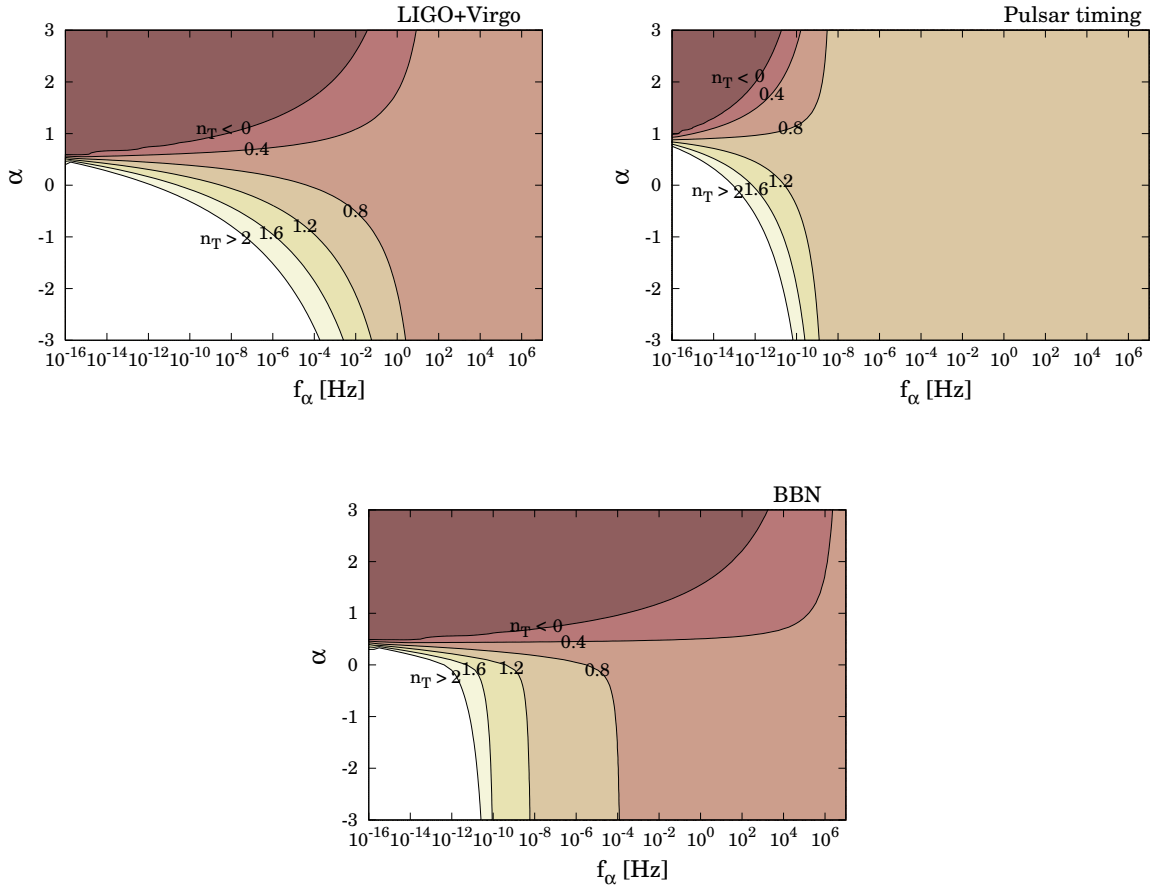


Figure 8: Contours of the  $2\sigma$  upper bound on  $n_T$  in the  $f_\alpha$ - $\alpha$  plane. Here  $r = 0.2$  is assumed.

## 4 Conclusion

We have provided more general constraints on the blue-tilted GW spectrum using observational bounds from LIGO, pulsar timing and BBN, taking into account the effect of the thermal history after inflation, such as reheating and late-time entropy production. The recent finding of CMB B-mode polarization by BICEP2 suggests the large tensor-to-scalar ratio  $r \sim 0.2$  and some analysis pointed out that the data favors a blue-tilted spectrum. Besides, from the theoretical point of view, there are several models of the early Universe which predict a blue-tilted spectrum, hence it is worth investigating to what extent blue-tilted spectrum can be allowed by current observational bound on the stochastic GW amplitude.

First, we have found that the suppression of the GW spectrum due to reheating can significantly relax the constraint on the tensor spectral index  $n_T$ , depending on the reheating temperature  $T_R$ . We have also shown that, by taking into account the late-time entropy production, the constraint on  $n_T$  changes depending on the amount of the produced entropy  $F$  and the cosmic temperature at the epoch of entropy production  $T_\sigma$ . When one does not take into account the thermal history (or assuming a very high reheating temperature such as  $T_R = 10^{15}$  GeV) and assume that the spectral amplitude continue to increase at high frequencies with the spectral index  $n_T$ , the constraints on  $n_T$  from BBN, LIGO and pulsar timing are  $n_T < 0.43$ , 0.54 and 0.87 for  $r = 0.2$  at 95 % C.L., respectively. These bounds are modified depending on the assumption of the thermal history: for example, if we consider reheating with  $T_R = 10^6$  GeV, these bound are weakened to  $n_T < 0.64$  (BBN), 0.89 (LIGO) and 0.87 (pulsar). If we consider a late-time entropy production after reheating with  $F = 10^2$ ,  $T_\sigma = 10^{-2}$  GeV and  $T_R = 10^{15}$  GeV, the bounds become  $n_T < 0.55$  (BBN), 0.68 (LIGO) and 1.1 (pulsar). Note that the results shown in this paper are all calculated assuming  $r = 0.2$ , motivated by the recent BICEP2 result. These bound on  $n_T$  changes for different values of  $r$ . Since  $r$  and  $n_T$  are degenerate in the expression of the spectrum as  $\Omega_{\text{GW}} \propto r(k/k_{\text{ref}})^{n_T}$ , the constraints on  $n_T$  are relaxed for small value of  $r$ , while the dependencies on the thermal history parameters are the same. The degree of the relaxation is determined by the value of  $k/k_{\text{ref}}$ , which has a different value depending on the experiment.

We have also discussed the constraints using the more generalized modeling of the spectrum, where the spectral power dependence changes at the characteristic frequency  $f_\alpha$  and we allow a general power-law form for the spectrum for  $f > f_\alpha$ . This modeling accommodates various models of the early Universe. We have shown that a significantly blue-tilted spectrum is still allowed in some parameter region, while there are also regions of parameter space where the value of  $n_T$  is severely constrained. Thus, the constraint on  $n_T$  strongly depends on the underlying models of the early Universe.

In this paper, we have demonstrated that a very blue-tilted GW spectrum can still be allowed in some particular models of the thermal history. However, in the future, various space-based interferometer experiments are planned, such as eLISA [57, 58], BBO [59, 60] and DECIGO [61] and so on. Once these experiments are realized, they will put a severe

constraint on the spectral index  $n_T$ , which would surely help to obtain new insight into the physics of the early Universe.

## Acknowledgments

The authors thank K. Nakayama and J. Yokoyama for helpful discussions. The work is supported by Grant-in-Aid for Scientific Research Nos. 24-2775 (SY) and 23740195 (TT) from the Ministry of Education, Culture, Sports, Science and Technology in Japan.

## A Analytic estimate of the BBN bound

Although we have numerically calculated the integral in the left hand side of Eq. (27) to obtain the BBN constraint in Sec. 3.2.1, here we show that the upper bounds on  $n_T$  can be analytically estimated and given in terms of reheating temperature  $T_R$ .

Assuming the standard thermal history after inflation, one can approximate the spectrum with a simple broken power-law such as

$$\Omega_{\text{GW}}(f) = \begin{cases} \Omega_{\text{GW}}(f_R) \left(\frac{f}{f_R}\right)^{n_T} & \text{for } f_{\text{eq}} < f_1 < f < f_R, \\ \Omega_{\text{GW}}(f_R) \left(\frac{f}{f_R}\right)^{n_T-2} & \text{for } f_R < f < f_2. \end{cases} \quad (31)$$

Then we can perform the integration in Eq. (27) and obtain

$$\frac{\Omega_{\text{GW}}(f_R)h^2}{n_T} \left[1 - \left(\frac{f_1}{f_R}\right)^{n_T}\right] + \frac{\Omega_{\text{GW}}(f_R)h^2}{2 - n_T} \left[1 - \left(\frac{f_2}{f_R}\right)^{n_T-2}\right] \leq 5.6 \times 10^{-6} (N_{\text{eff}}^{\text{upper}} - 3) \quad (32)$$

for  $0 < n_T < 2$ . Furthermore, in case with  $f_1 \ll f_R \ll f_2$ , we have a simple expression as

$$\Omega_{\text{GW}}(f_R)h^2 \leq \frac{n_T(2 - n_T)}{2} \times 5.6 \times 10^{-6} (N_{\text{eff}}^{\text{upper}} - 3). \quad (33)$$

Since one can also write down  $\Omega_{\text{GW}}(f_R)$  by using  $r, n_T$  and  $T_R$ , the above relation gives

$$\log\left(\frac{T_R}{10^6 \text{ GeV}}\right) < \frac{1}{n_T} \log(n_T(2 - n_T)) - 35.1 + \frac{24.3}{n_T} \simeq -35.1 + \frac{24.3}{n_T}, \quad (34)$$

where we have assumed  $k_{\text{ref}} = 0.01 \text{ Mpc}^{-1}$ ,  $g_* = 106.75$  and  $r = 0.2$ .

## References

- [1] P. A. R. Ade *et al.* [BICEP2 Collaboration], arXiv:1403.3985 [astro-ph.CO].
- [2] P. A. R. Ade *et al.* [BICEP2 Collaboration], arXiv:1403.4302 [astro-ph.CO].

- [3] H. Liu, P. Mertsch and S. Sarkar, arXiv:1404.1899 [astro-ph.CO].
- [4] M. J. Mortonson and U. Seljak, arXiv:1405.5857 [astro-ph.CO].
- [5] R. Flauger, J. C. Hill and D. N. Spergel, arXiv:1405.7351 [astro-ph.CO].
- [6] P. A. R. Ade *et al.* [Planck Collaboration], arXiv:1303.5082 [astro-ph.CO].
- [7] J. -O. Gong, arXiv:1403.5163 [astro-ph.CO].
- [8] M. Gerbino, A. Marchini, L. Pagano, L. Salvati, E. Di Valentino and A. Melchiorri, arXiv:1403.5732 [astro-ph.CO].
- [9] Y. Wang and W. Xue, arXiv:1403.5817 [astro-ph.CO].
- [10] A. Ashoorioon, K. Dimopoulos, M. M. Sheikh-Jabbari and G. Shiu, arXiv:1403.6099 [hep-th].
- [11] F. Wu, Y. Li, Y. Lu and X. Chen, arXiv:1403.6462 [astro-ph.CO].
- [12] R. H. Brandenberger, A. Nayeri, S. P. Patil and C. Vafa, Phys. Rev. Lett. **98**, 231302 (2007) [hep-th/0604126].
- [13] M. Baldi, F. Finelli and S. Matarrese, Phys. Rev. D **72**, 083504 (2005) [astro-ph/0505552].
- [14] T. Kobayashi, M. Yamaguchi and J. 'i. Yokoyama, Phys. Rev. Lett. **105**, 231302 (2010) [arXiv:1008.0603 [hep-th]].
- [15] G. Calcagni and S. Tsujikawa, Phys. Rev. D **70**, 103514 (2004) [astro-ph/0407543].
- [16] G. Calcagni, S. Kuroyanagi, J. Ohashi and S. Tsujikawa, JCAP **1403**, 052 (2014) [arXiv:1310.5186 [astro-ph.CO]].
- [17] J. L. Cook and L. Sorbo, Phys. Rev. D **85**, 023534 (2012) [Erratum-ibid. D **86**, 069901 (2012)] [arXiv:1109.0022 [astro-ph.CO]].
- [18] S. Mukohyama, R. Namba, M. Peloso and G. Shiu, arXiv:1405.0346 [astro-ph.CO].
- [19] F. A. Jenet, G. B. Hobbs, W. van Straten, R. N. Manchester, M. Bailes, J. P. W. Verbiest, R. T. Edwards and A. W. Hotan *et al.*, Astrophys. J. **653**, 1571 (2006) [astro-ph/0609013].
- [20] R. van Haasteren, Y. Levin, G. H. Janssen, K. Lazaridis, M. Kramer, B. W. Stappers, G. Desvignes and M. B. Purver *et al.*, Mon. Not. Roy. Astron. Soc. **414**, no. 4, 3117 (2011) [Erratum-ibid. **425**, no. 2, 1597 (2012)] [arXiv:1103.0576 [astro-ph.CO]].

- [21] P. B. Demorest, R. D. Ferdman, M. E. Gonzalez, D. Nice, S. Ransom, I. H. Stairs, Z. Arzoumanian and A. Brazier *et al.*, *Astrophys. J.* **762**, 94 (2013) [arXiv:1201.6641 [astro-ph.CO]].
- [22] W. Zhao, Y. Zhang, X. -P. You and Z. -H. Zhu, *Phys. Rev. D* **87**, 124012 (2013) [arXiv:1303.6718 [astro-ph.CO]].
- [23] B. Allen, In \*Les Houches 1995, Relativistic gravitation and gravitational radiation\* 373-417 [gr-qc/9604033].
- [24] M. Maggiore, *Phys. Rept.* **331**, 283 (2000) [gr-qc/9909001].
- [25] J. Aasi *et al.* [LIGO Scientific and VIRGO Collaborations], arXiv:1406.4556 [gr-qc].
- [26] J. Abadie *et al.* [LIGO Scientific and Virgo Collaborations], *Phys. Rev. D* **85**, 122001 (2012) [arXiv:1112.5004 [gr-qc]].
- [27] N. Seto, *Phys. Rev. D* **73**, 063001 (2006) [gr-qc/0510067].
- [28] T. L. Smith, E. Pierpaoli and M. Kamionkowski, *Phys. Rev. Lett.* **97**, 021301 (2006) [astro-ph/0603144].
- [29] I. Sendra and T. L. Smith, *Phys. Rev. D* **85**, 123002 (2012) [arXiv:1203.4232 [astro-ph.CO]].
- [30] A. Ota, T. Takahashi, H. Tashiro and M. Yamaguchi, arXiv:1406.0451 [astro-ph.CO].
- [31] J. Chluba, L. Dai, D. Grin, M. Amin and M. Kamionkowski, arXiv:1407.3653 [astro-ph.CO].
- [32] D. M. Siegel and M. Roth, *Astrophys. J.* **784**, 88 (2014) [arXiv:1401.6888 [gr-qc]].
- [33] J. W. Armstrong, L. Iess, P. Tortora and B. Bertotti, *Astrophys. J.* **599**, 806 (2003).
- [34] L. Hui, S. T. McWilliams and I-S. Yang, *Phys. Rev. D* **87**, 084009 (2013) [arXiv:1212.2623 [gr-qc]].
- [35] A. Shoda, M. Ando, K. Ishidoshiro, K. Okada, W. Kokuyama, Y. Aso and K. Tsubono, *Phys. Rev. D* **89**, 027101 (2014) [arXiv:1311.4273 [gr-qc]].
- [36] M. Coughlin and J. Harms, *Phys. Rev. Lett.* **112**, 101102 (2014) [arXiv:1401.3028 [gr-qc]].
- [37] T. Akutsu, S. Kawamura, A. Nishizawa, K. Arai, K. Yamamoto, D. Tatsumi, S. Nagano and E. Nishida *et al.*, *Phys. Rev. Lett.* **101**, 101101 (2008) [arXiv:0803.4094 [gr-qc]].

- [38] P. Astone, M. Bassan, P. Bonifazi, P. Carelli, C. Cosmelli, E. Coccia, V. Fafone and S. Frasca *et al.*, *Astron. Astrophys.* **351**, 811 (1999)
- [39] S. Aoyama, R. Tazai and K. Ichiki, arXiv:1402.4521 [gr-qc].
- [40] A. Stewart and R. Brandenberger, *JCAP* **0808**, 012 (2008) [arXiv:0711.4602 [astro-ph]].
- [41] R. Camerini, R. Durrer, A. Melchiorri, A. Riotto, *Phys. Rev. D* **77**, 101301 (2008) [arXiv:0802.1442 [astro-ph]].
- [42] N. Seto and J. 'I. Yokoyama, *J. Phys. Soc. Jap.* **72**, 3082 (2003) [gr-qc/0305096].
- [43] L. A. Boyle and A. Buonanno, *Phys. Rev. D* **78**, 043531 (2008) [arXiv:0708.2279 [astro-ph]].
- [44] K. Nakayama, S. Saito, Y. Suwa and J. 'i. Yokoyama, *Phys. Rev. D* **77**, 124001 (2008) [arXiv:0802.2452 [hep-ph]].
- [45] K. Nakayama, S. Saito, Y. Suwa and J. 'i. Yokoyama, *JCAP* **0806**, 020 (2008) [arXiv:0804.1827 [astro-ph]].
- [46] S. Kuroyanagi, T. Chiba and N. Sugiyama, *Phys. Rev. D* **79**, 103501 (2009) [arXiv:0804.3249 [astro-ph]].
- [47] S. Kuroyanagi, C. Gordon, J. Silk and N. Sugiyama, *Phys. Rev. D* **81**, 083524 (2010) [Erratum-ibid. *D* **82**, 069901 (2010)] [arXiv:0912.3683 [astro-ph.CO]].
- [48] K. Nakayama and J. 'i. Yokoyama, *JCAP* **1001**, 010 (2010) [arXiv:0910.0715 [astro-ph.CO]].
- [49] S. Kuroyanagi, K. Nakayama and S. Saito, *Phys. Rev. D* **84**, 123513 (2011) [arXiv:1110.4169 [astro-ph.CO]].
- [50] S. Kuroyanagi, C. Ringeval and T. Takahashi, *Phys. Rev. D* **87**, 083502 (2013) [arXiv:1301.1778 [astro-ph.CO]].
- [51] M. S. Turner, M. J. White and J. E. Lidsey, *Phys. Rev. D* **48**, 4613 (1993) [astro-ph/9306029].
- [52] S. Chongchitnan and G. Efstathiou, *Phys. Rev. D* **73**, 083511 (2006) [astro-ph/0602594].
- [53] Y. Watanabe and E. Komatsu, *Phys. Rev. D* **73**, 123515 (2006) [astro-ph/0604176].
- [54] L. E. Mendes and A. R. Liddle, gr-qc/9811040.

- [55] G. Steigman, *Adv. High Energy Phys.* **2012**, 268321 (2012) [arXiv:1208.0032 [hep-ph]].
- [56] H. Tashiro, T. Chiba and M. Sasaki, *Class. Quant. Grav.* **21**, 1761 (2004) [gr-qc/0307068].
- [57] P. Amaro-Seoane, S. Aoudia, S. Babak, P. Binetruy, E. Berti, A. Bohe, C. Caprini and M. Colpi *et al.*, arXiv:1201.3621 [astro-ph.CO].
- [58] P. Amaro-Seoane, S. Aoudia, S. Babak, P. Binetruy, E. Berti, A. Bohe, C. Caprini and M. Colpi *et al.*, *Class. Quant. Grav.* **29**, 124016 (2012) [arXiv:1202.0839 [gr-qc]].
- [59] S. Phinney *et al.*, *The big bang observer: direct detection of gravitational waves from the birth of the Universe to the present*, NASA Mission Concept Study.
- [60] G. M. Harry, P. Fritschel, D. A. Shaddock, W. Folkner and E. S. Phinney, *Class. Quant. Grav.* **23**, 4887 (2006) [Erratum-*ibid.* **23**, 7361 (2006)].
- [61] S. Kawamura, M. Ando, N. Seto, S. Sato, T. Nakamura, K. Tsubono, N. Kanda and T. Tanaka *et al.*, *Class. Quant. Grav.* **28**, 094011 (2011).